energies

MDPI

Article

Enhanced Seismic Protection System for an Emergency Diesel Generator Unit

Ricardo Bustamante [1], Gilberto Mosqueda [1,*] and Minkyu Kim [2]

[1] Department of Structural Engineering, University of California San Diego, La Jolla, CA 92093, USA; ribustam@eng.ucsd.edu
[2] Korea Atomic Energy Research Institute, Daedeok-Daero 989-111, Yusung-gu, Daejon 305-353, Korea; minkyu@kaeri.re.kr
* Correspondence: gmosqueda@eng.ucsd.edu

Abstract: Nuclear power plants are required to maintain operation after an earthquake, leading to a safe shutdown if necessary. In the case of a loss of offsite power, the onsite emergency diesel generator is critical to ensure procedural operations of the nuclear power plant. As a means to reduce the overall seismic risk, a three-dimensional seismic protection system is proposed to enhance the seismic performance of the emergency diesel generator. The proposed seismic isolation system decouples the horizontal and vertical components of shaking and considers available hardware to achieve an effective isolation solution over the range of excitation frequencies considered. Numerical analysis of the proposed system demonstrates a reduction in seismic demands on the emergency diesel generator and provides a higher safety margin than conventional base installation procedures. Umbilical lines that cross the isolation plane are considered and impose additional constraints on the displacement capacity of the isolation system. However, increasing the displacement capacity of these components can significantly increase the safety margin against failure. The seismic protection system can be customized depending on the seismic hazard and application to different seismic regions.

Keywords: base isolation; 3D seismic protection; nuclear power plant; emergency diesel generator; limit states; SPRA; HCLPF; fragility curves

Citation: Bustamante, R.; Mosqueda, G.; Kim, M. Enhanced Seismic Protection System for an Emergency Diesel Generator Unit. *Energies* **2022**, *15*, 1728. https://doi.org/10.3390/en15051728

Academic Editors: Guglielmo Lomonaco and Dan Gabriel Cacuci

Received: 19 January 2022
Accepted: 21 February 2022
Published: 25 February 2022

1. Introduction

The application of base isolation to equipment and nonstructural components has been studied for almost three decades [1–5]. Many proposed systems are adapted versions of non-seismic vibration isolation systems designed to limit the lateral travel of equipment. Most previous systems studied are composed of vertical coil springs with viscous dampers or restrainers in multiple directions. Nuclear power plants (NPPs) have several nonstructural components and equipment with different sizes, weights, and stiffnesses. Therefore, no unique and customizable three-dimensional (3D) isolation device has been studied that could simultaneously satisfy the seismic design requirements for the various medium-weight equipment and their sensitivity to base shaking.

Several studies have examined 3D seismic protection systems in NPPs [5–11]. Base isolation has been typically used to reduce the horizontal seismic demand, successfully applying it at the component level or for the whole structure to reduce acceleration. Different approaches have been used for the vertical seismic demand, ranging from springs to dampers and a combination of both. The type of approach depends on how the horizontal isolation is considered. Najafijozani et al. [5] studied adaptative vertical isolation of lightweight acceleration-sensitive equipment for a base-isolated NPP. Using a combination of springs and dampers, they achieved a reduction of the acceleration to meet the seismic capacity of the equipment. They focused solely on the vertical movement of the equipment, assuming the base isolation system of the NPP reduces the horizontal acceleration and suppresses any rocking. Medel-Vera and Ji [7] concluded that horizontally isolated structures

with vertical isolation at the equipment level avoid issues with the rocking motion and that it is more feasible to isolate lighter components vertically.

The emergency diesel generator (EDG) unit is typically located outside the NPP buildings, so any seismic protection system should isolate the unit horizontally and vertically. In a shake table test, Choeun et al. [12] studied the EDG performance supported by a coil spring–damper unit under two different types of ground motion. They found that the performance varied significantly with each ground motion set. The effectiveness depended on the natural frequency resulting from the coil springs and the ground motion frequency content. Nawrotzki and Siepe [11] studied the performance of helical springs and viscous dampers to implement a 3D protection system. Combining both allows to lower the fundamental frequencies and increase the structural damping.

This study focuses on the seismic protection of an emergency diesel generator, for which functionality is critical for the safe operation of NPP in a loss of offsite power (LOOP) event [13]. The proposed system is based on a combination of previously studied and widely applied devices such as lead rubber bearings (LRB) and vertical coil springs and dampers, merging their advantages to meet operational and seismic requirements. Notably, past experimental studies of LRB alone have indicated their effectiveness for horizontal motion isolation with the potential for amplification of vertical vibrations, including for NPPs [6]. The proposed 3D isolation system for the EDG comprises lead rubber bearings (LRB) to isolate the horizontal ground shaking. A spring and damper vibration isolation layer is included as a second isolation layer on top of the LRB system to mitigate the effect of vertical shaking. A similar approach has been proposed to isolate lightweight equipment in NPPs [5] and for building structures [14,15].

The proposed 3D isolation system is designed for a generic medium-weight EDG, and seismic probabilistic risk analysis (SPRA) is performed. An incremental dynamic analysis (IDA) [16] is performed to obtain fragility curves [17] for two distinct engineering demand parameters (EDP). The common EDP for a non-isolated EDG unit is acceleration [12]. In contrast, an additional EDP is required to control the isolation system lateral displacement for an isolated EDG unit. This study considers two displacement-based failure criteria: the bearings lateral deformation and the umbilical lines deformation capacity crossing the isolation interface. The SPRA as applied in this study is limited to a few ground motions, focusing on demonstrating the feasibility of the design. Rocking is not allowed in the numerical model. It is assumed that an adequate frictionless rocking restraint system with vertical guides is provided following commercially available 3D isolation systems [18].

The proposed seismic protection system can be customized for different sizes, weights, and seismic hazards. Fragility functions characterize the current system and identify the high confidence of a low probability of failure of key components.

2. Seismic Hazard and Expected Seismic Performance

The proposed design of the EDG is based on a set of synthetic seismic input ground motions compatible with a uniform hazard spectra (UHS). Five three-dimensional ground motion sets are generated based on the UHS (10^{-4}/year) for Uljin, South Korea with a PGA = 0.273 g [19,20]. Figure 1 shows the target pseudospectral acceleration for the horizontal and vertical directions with the individual ground motions shown in a lighter shade. The artificial motions provided closely follow the target spectra, showing low variability among them.

The hazard exceedance probability (H_D) for the ground motions as provided is equivalent to a Seismic Design Category 5 (SDC-5) according to ASCE/SEI-43-05 [21]. This probability of exceedance has a qualitative goal related to acceptable structural behavior or limit state (LS). The limit states are specified from LS-A when large deformation and significant damage are accepted to LS-D, when no damage and elastic behavior are expected. For this study, the limit state considered is LS-D, i.e., no damage and linear behavior are expected.

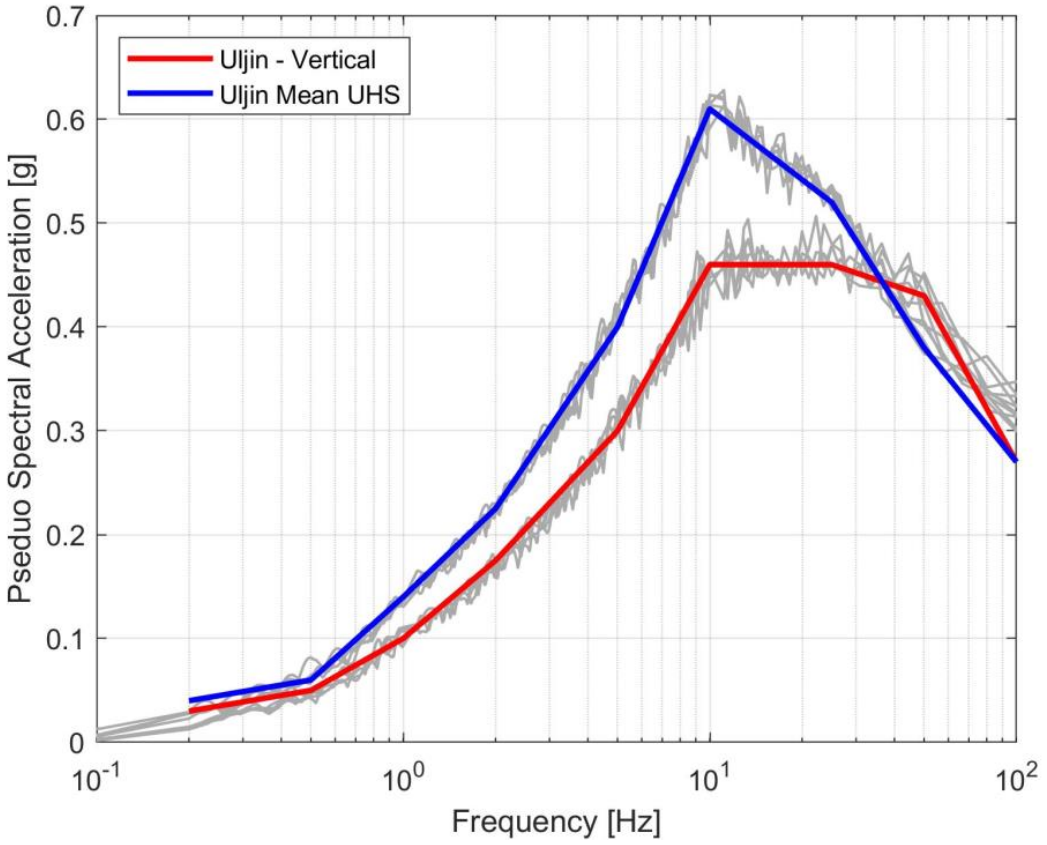

Figure 1. Ground motion pseudospectral acceleration.

The selected limit state LS-D can be related to a prefailure mode of the primary components of an EDG system. Structural failure modes can result from the equipment frame, the anchorage system, or the umbilical lines. The seismic probabilistic assessment is based on fragility curves following NUREG [22,23]. The safety margin is obtained after expressing the capacity in terms of the high confidence of a low probability of failure (HCLPF), defined as "the acceleration value for which we have approximately 95% confidence that the probability of failure is less than about 5%" [22]. This HCLPF value represents the equipment or component capacity that corresponds to the earthquake level at which it is unlikely that failure will occur. The earthquake level is typically expressed in terms of the peak ground acceleration (PGA), defined as the average of the two horizontal peak components of free-field ground-surface acceleration.

The seismic performance of the equipment is evaluated using two engineering demand parameters (EDPs). The probability of failure of the EDG unit can be characterized by the acceleration experienced by the unit, while the base isolation system and the umbilicals crossing the isolation plane are characterized by their displacement capacity. Therefore, two different types of HCLPF capacities are examined: the first based on the isolation system lateral deformation and the second based on the EDG acceleration. Previous studies [7–11,24] have provided the parameters to estimate the HCLPF value for the EDG unit, the anchorage, and the umbilical lines attached to the EDG. Parameters reported include the median capacity and the randomness and uncertainty standard deviations. Table 1 summarizes the HCLPF values per EDP found in the literature.

Table 1. Limit states and HCLPF values per EDP.

EDP	Label	Limit State	Value	Reference
EDG Acceleration	DS1-A	EDG LS1	0.40 g	[25]
Isolation Lateral Displacement	DS1-D	Pipeline LS1	127 mm	[26]
	DS2-D	Bearing LS2	320 mm (γ_s = 250%)	[27]
	DS3-D	Bearing LS3	576 mm (γ_s = 450%)	[27]

The HCLPF values for the EDG isolation lateral displacement limit states are defined for two components. One component is the pipeline attached to the EDG that crosses the isolation interface. In a standard piping system, seismic demands lead to plastic deformation and potential failure in the elbows of the piping system [28,29]. Jeon et al. [26] provide seismic fragility curves for elbows in piping systems expressed in terms of the maximum relative displacement between the ground and the isolated floor. This displacement is defined as 1D in an analysis that does not consider the vertical ground motion and uses a standard pipeline system. Due to limited data on 3D base-isolated NPP piping systems, the 1D relative displacement is considered in this study, using the 127 mm value for the horizontal relative displacement. A flexible pipeline designed to accommodate the relative displacement could provide a larger deformation capacity.

The second component of the isolation lateral displacement EDP is the bearings. The bearing limit state is expressed in terms of the shear strain deformation. The bearing vertical load capacity is assumed to be checked in the design process.

The HCLPF value for the EDG acceleration limit state is based on the PGA for non-isolated EDG unit studies. The value chosen to represent the EDG acceleration EDP characterizes the functional and structural failure of the non-isolated EDG unit [25]. Structural failure refers to anchor bolt failure, breakout, tension, or shear failure. Choun and Kim [30] reported that the expected failure mode of an EDG is due to concrete coning with an HCLPF equal to 0.38 g. The acceleration used to characterize the HCLPF is for the ground level and does not necessarily equal the acceleration experienced by the EDG unit. Kawakami et al. [31] reports a 1.2 amplification factor from the PGA to the EDG acceleration.

Placing the EDG unit on 3D seismic isolation can reduce the accelerations experienced by the EDG and increase the limit state value in terms of PGA. In this study, a conservative approach is taken by considering the allowable acceleration on the EDG unit to equal the previously reported PGA values for HCLPF. It should be noted that experimental studies on isolated and conventionally supported EDGs are limited to better characterize the level of amplification in both cases. Further, there are no reports of limit state for vertical excitation of EDG within the literature. It is assumed that the EDG unit can withstand the vertical seismic demands if the 3D isolation system can reduce the transmissibility of accelerations from the ground to the EDG.

3. Design of Seismic Protection System

For the design of the 3D seismic isolation system, a simplified model of the EDG is considered. The EDG is assumed to have a weight equal to 150 Tf and a primary vibration frequency of 34 Hz following [3]. The analyses models consider the EDG as a single degree of freedom with lumped mass at mid-height of the EDG unit.

Different seismic protection configurations were examined. The proposed seismic protection presented here can reduce the EDG acceleration and limit the lateral displacement. The layout is based on two physical levels of isolation. The bottom level (*IsoH*) consists of six lead rubber bearings (LRBs), while the top level (*IsoV*) consists of 12 coil springs and viscous dampers units. A rigid frame is considered between the two isolation levels. Figure 2 shows the proposed configuration.

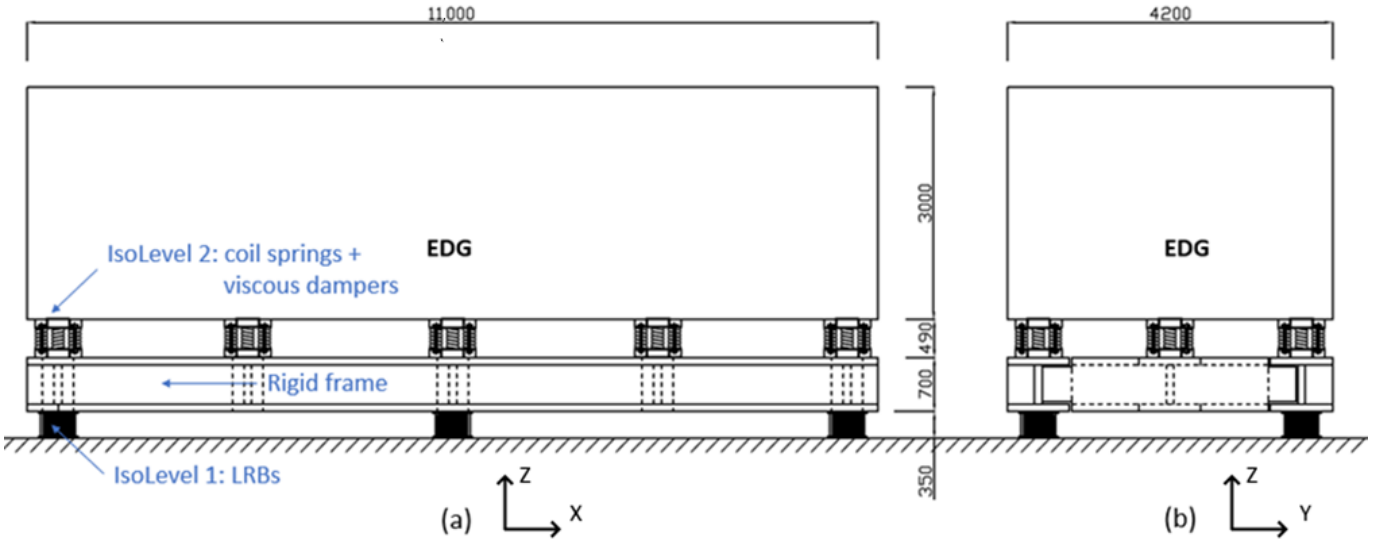

Figure 2. Proposed seismic protection configuration: (**a**) side elevation view; (**b**) front elevation view. Dimensions in millimeters.

Each isolation level targets the reduction of the seismic demand in a particular direction. *IsoH* focuses solely on the horizontal plane, while *IsoV* on the vertical axis. The decoupling allows for customization of the devices based on the seismic hazard, including the frequency content. This feature could enable simple adjustments to standardize its use for different seismic regions.

The frequency content of the seismic hazard considered shows a peak around 11 Hz for the horizontal plane and a plateau between 8 Hz and 20 Hz for the vertical component. This information is used to define the properties of both isolation levels, such that the primary vibration frequency of each level is below the peak frequencies of the seismic hazard.

Lead rubber bearings are considered and sized to define the *IsoH* frequencies. Lead rubber bearings typically result in a lower natural vibration frequency in the horizontal plane, typically around 0.25 Hz to 1.0 Hz, and a higher frequency in the vertical axis of about 10 Hz and higher. The *IsoV* frequencies are defined by the coil springs. The vibration control performance defines restrictions for the vertical natural frequency of the coil spring [32]. Providing a low natural vertical frequency is beneficial for the seismic demand but sets the spring static deflection to be large which is detrimental during operation. The performance during normal operation is critical; hence, the static deflection defines the vertical frequency. Following [32], the coil spring vertical frequency is set to 2.0 Hz which defines a static deflection equal to 62 mm. Table 2 summarizes the required vibration frequencies upon the primary frequency content of the ground motions.

Table 2. Frequency-dependent properties of both isolation levels.

Isolation Level	Horizontal Vibration Frequency (Hz)	Vertical Vibration Frequency (Hz)	Primary Horizontal Frequency (Hz)
IsoH	[0.25–4.0]	>10	11
IsoV	-	~2.0	[8–20]

The design of the horizontal isolation system considers a tradeoff between the transfer of shear forces related to the accelerations experienced by the EDG and the displacement demand for a given hazard level. This is demonstrated for the EDG and the considered seismic hazard following the equivalent lateral force procedure in FEMA P-751 [33], as shown in Figure 3.

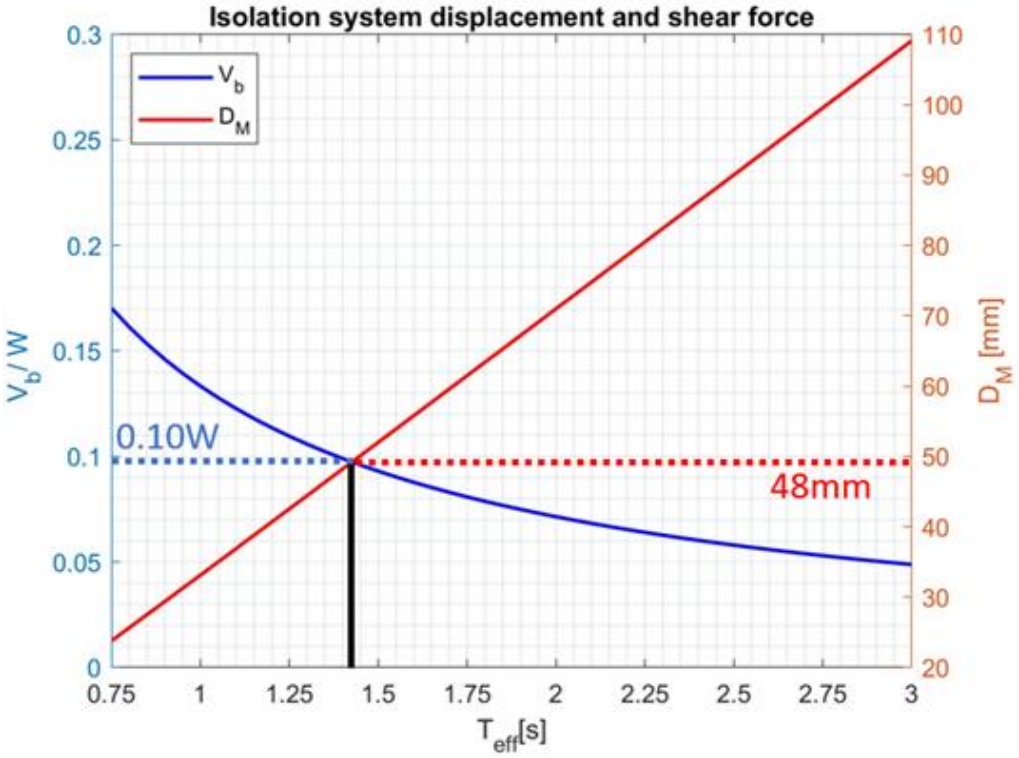

Figure 3. FEMA P-751 equivalent lateral force procedure results.

The effective period of the isolation systems is based on the linearization of the stiffness and damping of the inherently nonlinear bearings. The value chosen is the intersection of the base shear and the lateral displacement. This was found as a reasonable comprise to provide reduced base shear while limiting the horizontal displacement at a vibration frequency of 0.7 Hz (period of 1.40 s). To verify the feasibility of this design, the required bearings are sized with dimensions and resulting bearing properties for *IsoH* shown in Table 3.

Table 3. Properties of LRB and resulting isolation system properties.

Type	Diameter (mm)	Lead Core (mm)	Rubber Thickness (mm)	Shear Modulus (MPa)	Rubber Layers -	f_H (Hz)	f_V (Hz)
Lead Rubber	405	40	8	0.4	16	0.7	13.8

The equations and assumptions to obtain the horizontal and vertical effective properties of the LRB system are described considering a bilinear model for the bearings. The ratio between the horizontal elastic stiffness (k_1) and the post-yield stiffness (k_2) is 10. The post-yield stiffness of the laminated rubber bearings is expressed as

$$k_1 = 10k_2 \tag{1}$$

$$k_2 = \frac{G_{eff} \cdot (A_e - A_i)}{n_r \cdot t_r} \tag{2}$$

The yield force (Fy) and yield displacement (D_y) are obtained based on the characteristic strength of the lead (Q) and the horizontal elastic stiffness (k_1) and the post-yield stiffness (k_2).

$$F_y = \frac{Q \cdot k_1}{k_1 - k_2} \tag{3}$$

$$D_y = \frac{F_y}{k_1} \tag{4}$$

The energy dissipated (W_{eff}) can be expressed as

$$W_{eff} = 4 \cdot Q \cdot (D - D_y) \tag{5}$$

The effective horizontal stiffness ($k_{eff,H}$) and vertical stiffness ($k_{eff,V}$) values are obtained based on the lateral displacement (D), the effective rubber shear modulus (G), the external isolator area (A_e), internal area (A_i), the number of rubber layers (n_r), the rubber thickness for each layer (t_r), and the shim thickness (t_s) as [34–36] follows:

$$k_{eff,H} = \frac{Q}{D_{isp}} + \frac{G_{eff} \cdot (A_e - A_i)}{n_r \cdot t_r} \tag{6}$$

$$k_{eff,V} = \frac{(A_e - A_i) \cdot E_c}{n_r \cdot t_r + (n_r - 1) \cdot t_s} \tag{7}$$

with the compressive modulus (E_c) and shape factor (S) expressed as

$${E_c}^{-1} = \frac{1}{6G_{eff} \cdot S^2} + \frac{4}{3 \cdot K} \tag{8}$$

$$S = \frac{{D_e}^2 - {D_i}^2}{4 \cdot D_e \cdot t_r} \tag{9}$$

The coil springs in the *IsoV* level are sized for two conditions: the operational vibration (including vertical static deflection) and the primary vertical frequency content of the ground motion. The target is to achieve a primary vertical frequency less than 2 Hz, satisfying both conditions. The dampers are sized based upon a parametric study of a feasible range of sizes while targeting the reduction of the ground acceleration. A linear viscous damper with force proportional to velocity is used with the system properties shown in Table 4 including the % of critical damping.

Table 4. *IsoV* properties.

Type	Direction	Value	f (Hz)	Damping (%)
Stiffness	Horizontal	16.4 (kN/mm)	2.5	-
	Vertical	28.4 (kN/mm)	2.0	-
Damping coefficient	Horizontal	1.55 (kN s/mm)	-	12.0
	Vertical	5.37 (kN s/mm)	-	11.0

The vertical stiffness is defined using the targeted vertical frequency:

$$K_{ISO\ V} = 4\pi^2 \cdot m \cdot {f_v}^2 \tag{10}$$

The static deflection can be obtained as

$$\delta_0 = \frac{g}{4\pi^2 \cdot {f_v}^2} \tag{11}$$

A lumped mass is added to the numerical model to account for the rigid frame, and the *IsoV* weight is estimated as 30 (Tf). No rocking is allowed in the numerical model, assuming an adequate rocking restraint system with vertical guides for the *IsoV* layer. The analytical model is developed in OpenSees [37] structural analysis software.

4. Results

Nonlinear time-history analyses were conducted to examine the performance of the EDG under the five ground motion sets considered. The results are first presented for an individual ground motion to understand the isolation system's behavior and the EDG's response. Record 4 is selected since it is most representative of the average response of the five records. The record is applied at two scale factors, including the unscaled record with a PGA of 0.273 g, and scaled to a horizontal PGA of 0.925 g. The higher amplitude was selected as this is when the first potential limit state is reached, as shown in Table 1.

4.1. Response for Target Seismic Hazard Intensity

The unscaled Record 4 with a PGA of 0.273 g is used to demonstrate the performance of the 3D isolated EDG under the target UHS. The acceleration of each isolation level and the EDG unit are compared, both in the horizontal and vertical directions in Figures 4 and 5.

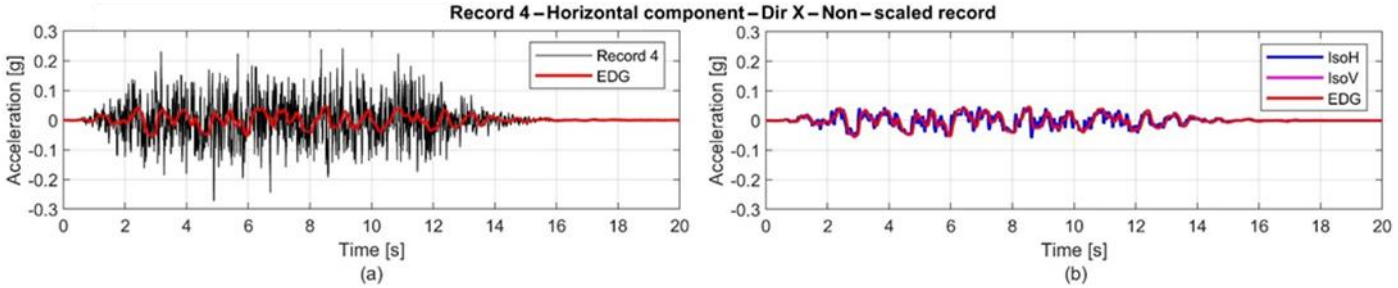

Figure 4. Horizontal acceleration time history results for non-scaled Record 4—direction "X". (**a**) Record and EDG response comparison; (**b**) System response by isolation level.

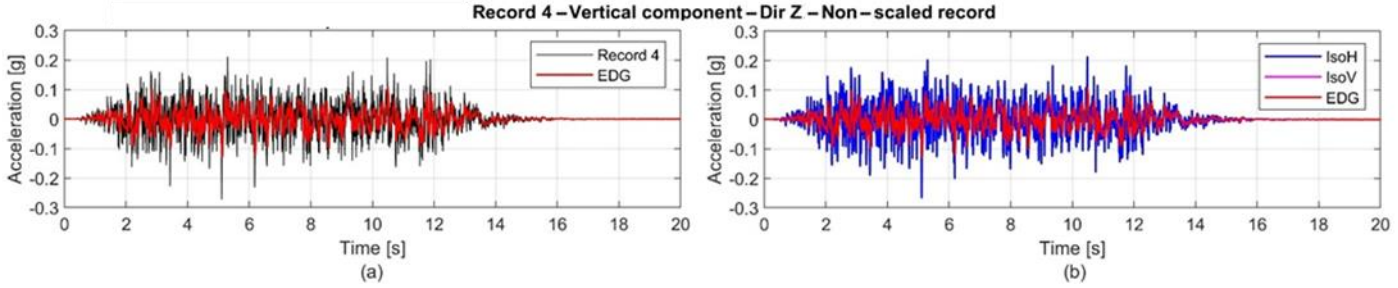

Figure 5. Vertical acceleration time history results for non-scaled Record 4—direction "Z". (**a**) Record and EDG response comparison; (**b**) System response by isolation level.

The horizontal acceleration time histories in the "X" direction are shown in Figure 4a. An amplification factor from the PGA to the EDG acceleration is used to quantify the proposed seismic protection system performance after Kawakami et al. [31], who reports a factor of 1.20 for the 2D ground motion, not providing a factor for the 3D ground motion. Considering only the 2D horizontal acceleration, a factor of 0.22 times the PGA is obtained, while a factor of 0.50 times the PGA is obtained for the 3D ground motion. Including the vertical ground motion reduces the effectiveness of the proposed seismic protection system, although still reducing the EDG acceleration for the unscaled ground motion set. The EDG acceleration time history shows that the proposed seismic protection system can filter the high-frequency content of the horizontal shaking. The acceleration time histories immediately above each isolation level and the EDG unit are shown in Figure 4b. Notably, the *IsoV* level further reduced the high-frequency content experienced above the *IsoH* level due to the additional contribution of the low horizontal stiffness provided by the coil springs. The EDG behaves as a rigid body, and thus its response is identical to the *IsoV* time histories, which is why the *IsoV* line is not visible.

The vertical input ground motion is compared to the EDG vertical acceleration in Figure 5a, indicating a reduction factor of about two while still transmitting the high-

frequency content. The vertical vibration frequencies of both isolation levels are close to the dominant range of the input ground motion, transmitting some of the high-frequency shaking into the EDG unit. Figure 5b shows the effects of the *IsoV* level defined by the coil springs in reducing the acceleration experienced by the EDG unit. The acceleration of the *IsoH* level is about the same as the vertical ground motion, showing that the LRB alone would not reduce the vertical response.

Figure 6 compares the pseudospectral acceleration (PSA) corresponding to 5% of critical damping for the ground record, the EDG, and above each isolation level for the horizontal and vertical directions. The horizontal PSA in Figure 6a has a marker to indicate the EDG unit natural frequency of 34 Hz corresponding to PSA = 0.056 g with the isolation system. The reduction in PSA is clearly shown above each isolation level. Figure 6a also confirms that the *IsoV* level further reduces the higher frequency vibration between 3–30 Hz, although it causes slight amplification in lower frequencies. The vertical PSA in Figure 6b indicates that *IsoH* amplifies the vertical ground motion across the LRB, a concept that has previously been raised for horizontal isolations systems [6], while *IsoV* effectively reduces the vertical excitation above 5 Hz.

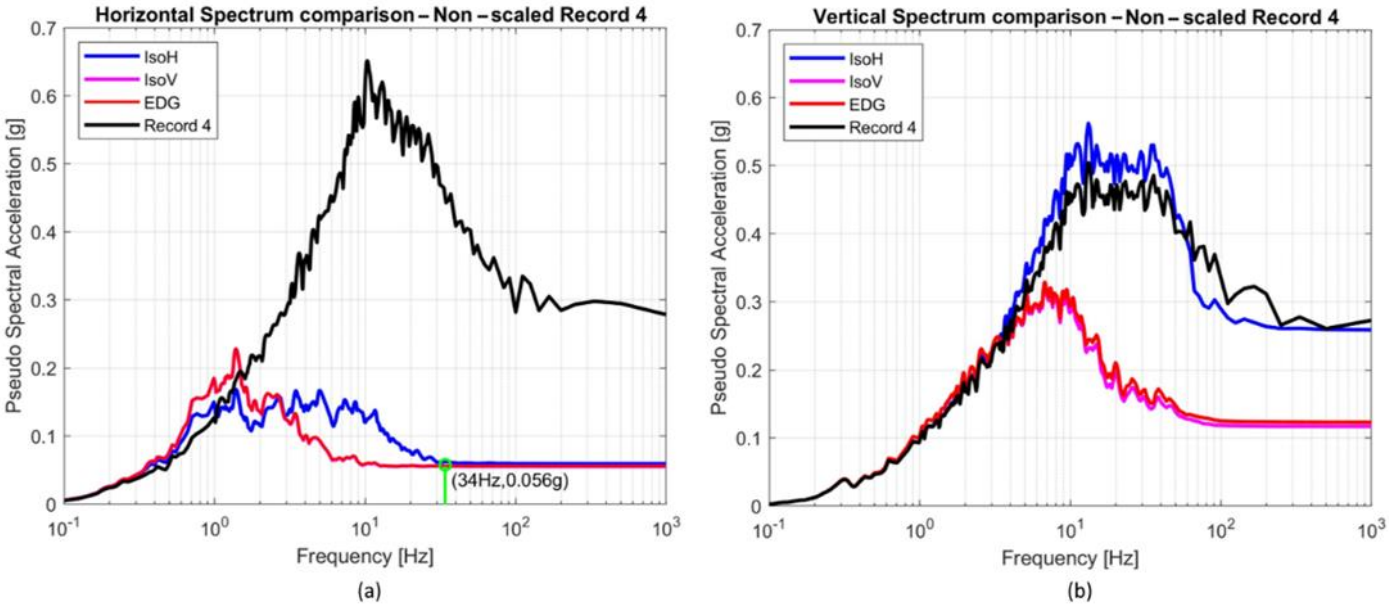

Figure 6. Spectral acceleration results for non-scaled Record 4. (**a**) Horizontal direction "X"; (**b**) Vertical direction "Z".

The results for Record 4 shown here are representative of the average response for the five considered records. These detailed results show the effectiveness of the proposed seismic protection system in reducing the seismic demands for a given seismic hazard as specified by the UHS.

The second EDP considered is the isolation system lateral displacement. The base isolation system and the umbilicals crossing the isolation plane are characterized by their displacement capacity. For the unscaled Record 4, the isolation system lateral displacement is about 15 mm, with the horizontal acceleration transferred to the base of the EDG reduced by a factor of 4.5 and the vertical acceleration reduced by a factor of 2. The small lateral displacement is expected for this seismic hazard with a high-frequency content. Different results are expected for seismic hazards with lower primary frequencies, which are considered in the next section.

4.2. Scaled Ground Motion Record

To observe the response of the seismically isolated EDG at a higher intensity, Record 4 is scaled to a horizontal PGA of 0.925 g, at which the isolation system lateral displacement

reaches the first limit state (LS1-D), corresponding to 127 mm at which the piping systems crossing the isolation plane reach its deformation capacity. The results in Figure 7 show a similar performance to the non-scaled record in Figure 4. In Figure 7a, the EDG horizontal acceleration is significantly reduced in amplitude while Figure 7b shows that the EDG unit experiences a 0.166 g acceleration with an isolation system lateral displacement equal to 127 mm for this scaled seismic hazard. A 2D horizontal acceleration factor of 0.18 times the PGA is obtained, while a factor of 0.48 times the PGA is obtained for the 3D ground motion. Notably, the reduced horizontal seismic demands are conditional on the deformation capacity of the pipeline crossing the isolation interface. The vertical isolation response shown in Figure 8 shows the same response observed for the non-scaled record. This type of response is expected since the vertical isolation is linear.

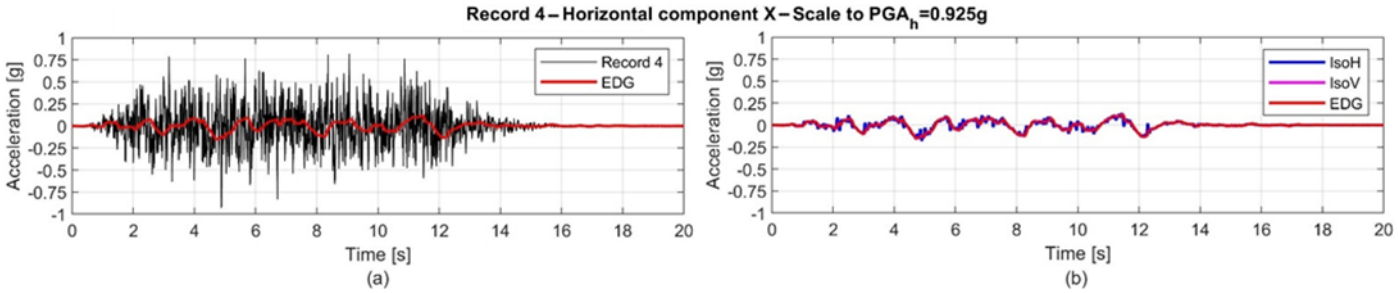

Figure 7. Horizontal acceleration time history results for Record 4 with PGA = 0.925 g—direction "X". (**a**) Record and EDG response comparison; (**b**) System response by isolation level.

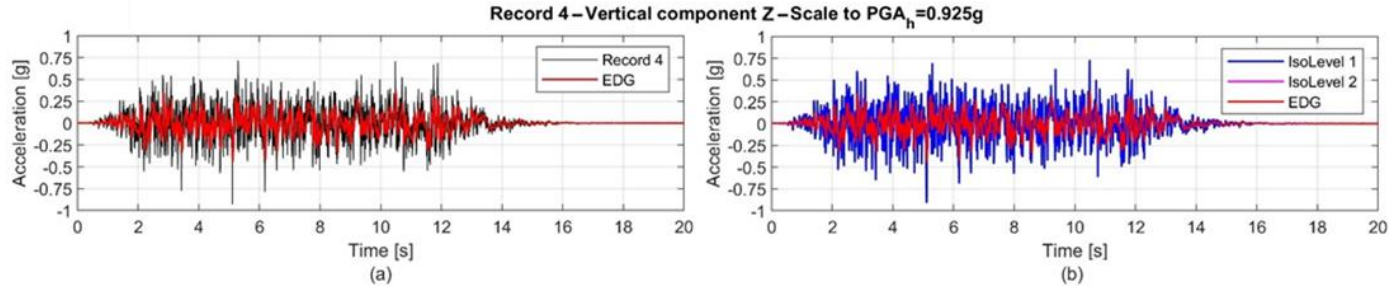

Figure 8. Vertical acceleration time history results for Record 4 with PGA = 0.925 g—direction "Z". (**a**) Record and EDG response comparison; (**b**) System response by isolation level.

The results shown in Figure 9 are similar to the results in Figure 6. The horizontal PSA in Figure 9a is significantly reduced for all isolation levels. The vertical PSA in Figure 9b shows a reduction of the EDG acceleration and amplification for the *IsoH* level. For this scaled record intensity, there is no amplitude dependence.

The behavior of the isolation systems is shown in Figure 10 for both horizontal and vertical directions. The individual force–displacement hysteretic behavior of levels *IsoV* and *IsoH* shows that most of the lateral deformation is captured by the LRB. The LRB bearings have a lower effective stiffness and dissipate energy through hysteretic action of the lead core while the coil springs have the added linear viscous dampers to dissipate energy. The force–displacement behavior in the vertical direction of the *IsoV* demonstrates that the response is dominated by the viscous dampers with small oscillations around the static deflection equal to 63 mm. The *IsoH* level in Figure 10d shows that the behavior of the bearing in the vertical direction is modeled as a linear spring with 2% damping not shown.

The time-history analysis for a single ground motion provides insight into the behavior of the isolation system. A more thorough probabilistic analysis is necessary to quantify the ground motion intensity at which there is a high confidence of a low probability of failure (HCLPF), as described in the next section.

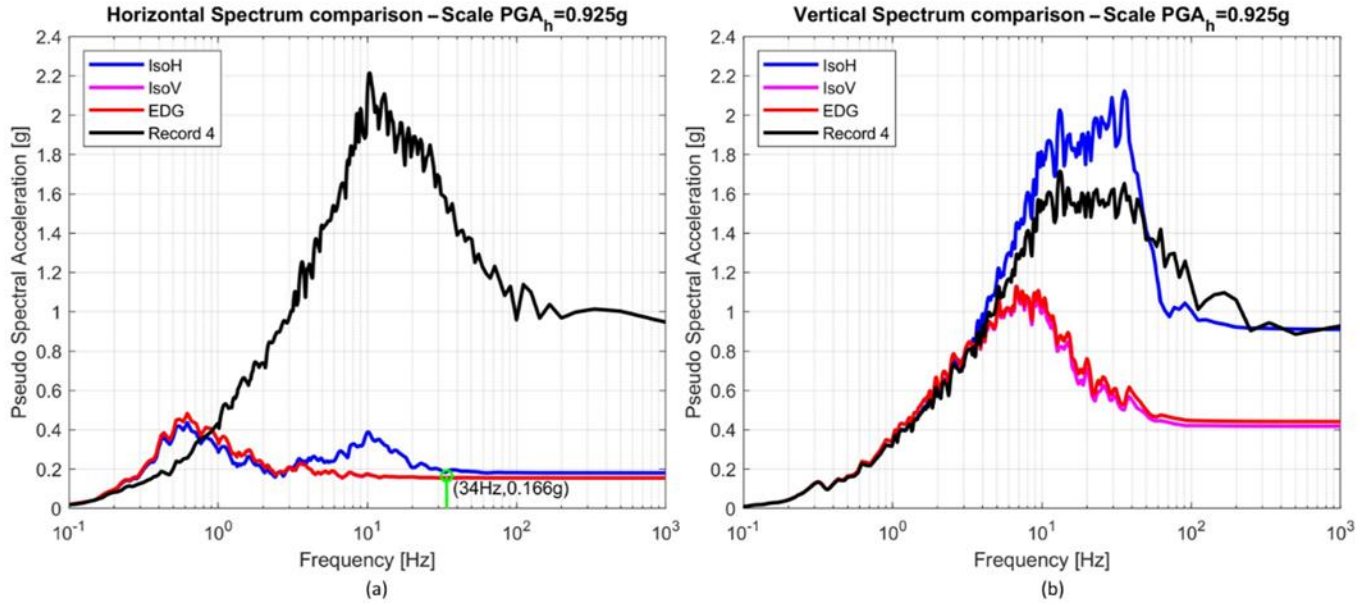

Figure 9. PSA results for the scaled Record 4. (**a**) Horizontal direction "X"; (**b**) Vertical direction "Z".

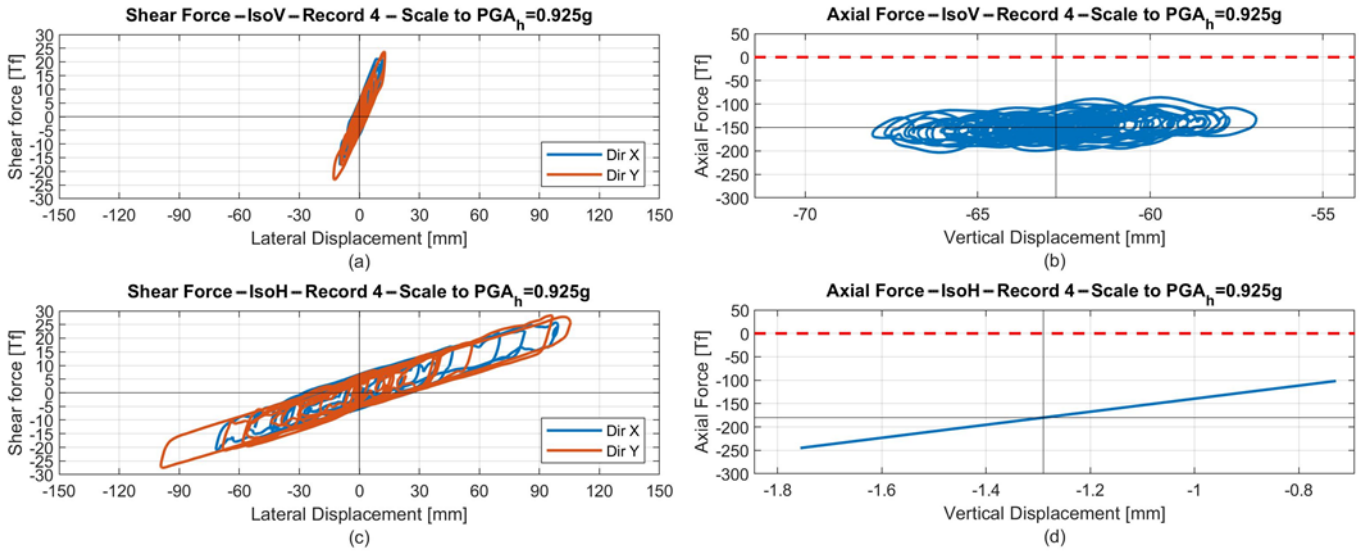

Figure 10. Force–displacement hysteresis for the scaled Record 4. (**a**) *IsoV* horizontal direction "X" response. (**b**) *IsoV* vertical direction "Z" response. (**c**) *IsoH* horizontal direction "X" response. (**d**) *IsoH* vertical direction "Z" response.

4.3. Incremental Dynamic Analysis

An incremental dynamic analysis (IDA) is a nonlinear dynamic analysis method that correlates the seismic demand and the capacity estimation using single or multiple ground motion records incrementally scaled in magnitude. The IDA is performed to derive fragility curves for two engineering demand parameters, including displacements at the isolation level and accelerations in the EDG. The limit states considered for each EDP are described in Table 1. The five ground motion triplets are used to account for seismic hazard randomness (β_R), while an uncertainty standard deviation (β_U) equal to 0.30 is assumed. The records are scaled from 0.1 to 10 times the original PGA, in increments of 0.1 g.

4.3.1. Base Isolation System Lateral Displacement

Figure 11 shows the IDA result for each ground motion's isolation system lateral displacement with the displacement limit state considered indicated by vertical dashed

lines. The horizontal axis is presented by the rubber bearings shear deformation, and the one at the bottom is expressed in terms of the maximum lateral deformation.

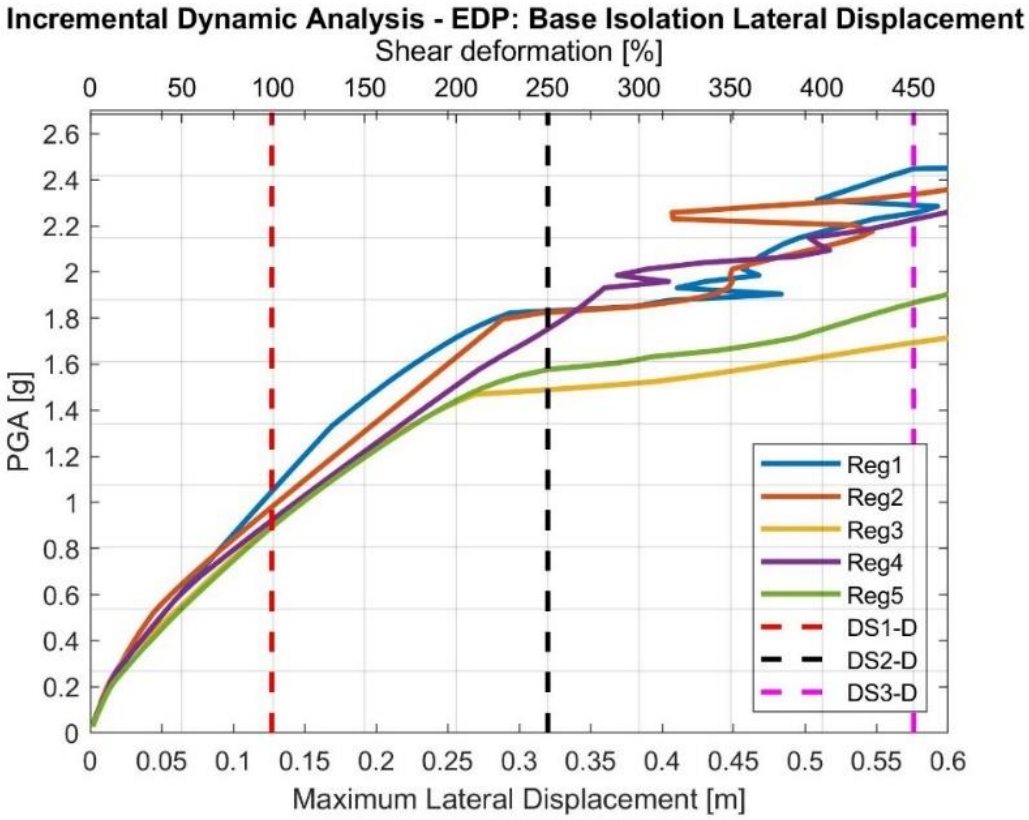

Figure 11. IDA for lateral displacement EDP.

Table 5 contains the median PGA and the randomness standard deviation value for each limit state. The resulting β_r values are relatively small, providing little variation in response between the ground motions. This is likely the result of the scaling method used for the ground motion to closely match the desired spectrum.

Table 5. IDA results for the lateral displacement EDP.

EDP	Label	Limit State	Value (mm)	Median PGA (g)	β_R
Isolation Lateral Displacement	DS1-D	Pipeline LS1	127	0.94	0.07
	DS2-D	Bearing LS2	320	1.75	0.10
	DS3-D	Bearing LS3	576	2.23	0.17

4.3.2. EDG Acceleration

The results for the EDG acceleration limit state are provided in a similar format in Figure 12. The values in Table 6 contain the median PGA and the randomness standard deviation value for EDG acceleration limit state.

Table 6. IDA results for the EDG acceleration EDP.

EDP	Label	Limit State	Value (g)	Median PGA (g)	β_R
EDG Acceleration	DS1-A	EDG LS1	0.40	1.80	0.07

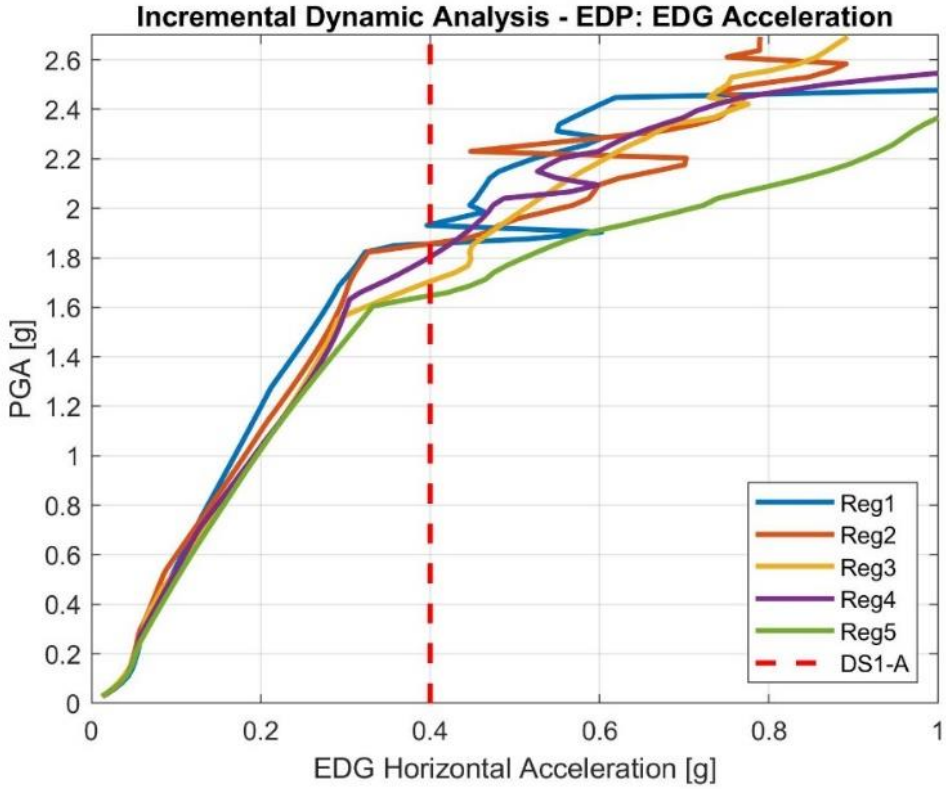

Figure 12. IDA for EDG acceleration EDP.

4.4. Fragility Curves

Fragility curves estimate the probability of obtaining damage levels or grades as a function of each the seismic hazard intensities. The application of fragility curves on nonstructural elements [38,39] and other fields [40] is extensive. The fragility curves considered are used to calculate the probability of exceeding a specific limit state for a given ground motion PGA. The median fragility curve is obtained directly from the IDA data, while the 95% curve is the 95% confidence that the median capacity exceeds the PGA level. The HCLPF value is obtained at a 5% failure probability of the 95% confidence probability distribution.

The fragility curves are based on three parameters, including the median capacity and the logarithmic standard deviation representing random uncertainty obtained directly from the IDA and listed in Tables 5 and 6. The third parameter is the uncertainty logarithmic standard deviation (β_u), representing systematic or modeling uncertainty. The value assumed for all cases is $\beta_u = 0.30$.

4.4.1. Base Isolation System Lateral Displacement

The median and 95% confidence probability distribution curves for all the displacement-based limit states are plotted in Figure 13. For the first displacement-based limit state, i.e., the pipeline LS1 in Figure 13a, the HCLPF value is 0.50 g, represented by the blue dashed line. The EDG unit could experience a ground motion similar to the UHS described in Figure 1 with a 5% probability of failure. This failure comes from the assumption of exceeding the lateral deformation capacity of the pipeline crossing the isolation interface. Figure 13b shows that the HCLPF value for the bearing LS2 is 0.91 g. This particular limit state is related to the bearing reaching a shear deformation of 250%, which is defined as a limit for the bearing's linear behavior [27]. Exceeding this shear deformation threshold does not imply a bearing failure; rather, highly nonlinear behavior is expected in the rubber that could include stiffening. Figure 13c shows that the HCLPF value for the bearing LS3 is 1.03 g. This lateral deformation is equivalent to a 450% bearing shear strain, defined as a

fracture limit [27]. Changes in the bearing design can lead to higher lateral displacements by changing the bearing diameter, the number, and the thickness of the rubber layers.

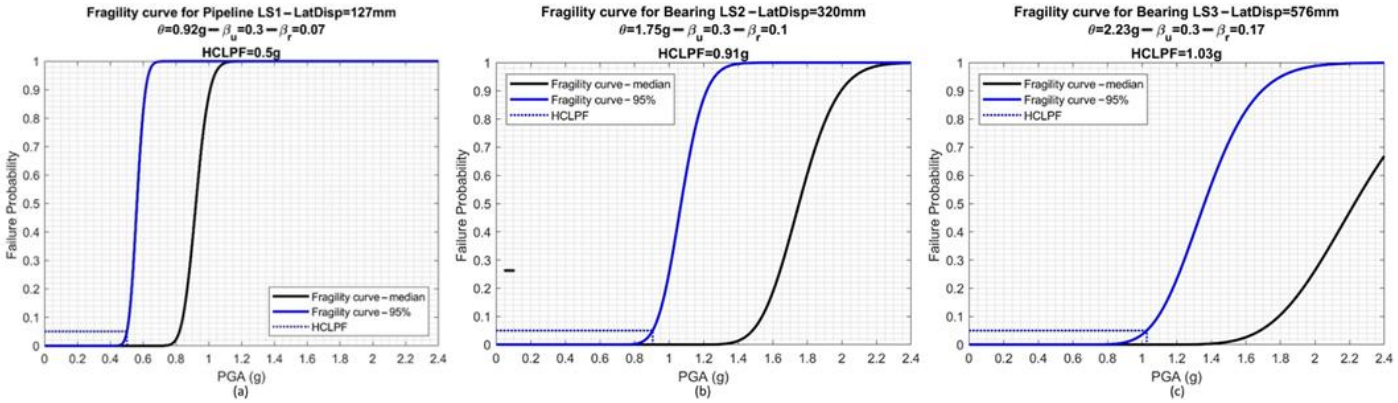

Figure 13. Fragility curve for (**a**) pipeline LS1, (**b**) bearing LS2—LatDisp = 320 mm, and (**c**) bearing LS3—LatDisp = 576 mm.

The fragility curves for the base isolation system lateral displacement EDP show a significant difference in the deformation capacity of the components crossing the isolation interface. The bearings can sustain a larger deformation than the pipeline before exhibiting damage. To take advantage of the bearing's deformation capacity, umbilicals crossing the isolation interface can be designed to accommodate larger deformations, as is typically done in buildings. This would enhance the system's performance and allow it to sustain higher seismic demands.

4.4.2. EDG Acceleration

The values in Table 6 are used to develop the fragility curves for the three acceleration limit states. These limit states are based on reported values of non-isolated EDG units, specifically to the failure modes these units experience. The conservative assumption made here is that since the EDG unit is assumed to be rigid, the reported PGA should be similar to the EDG acceleration [31]. The behavior of an isolated EDG unit is unknown, and it is believed that some failure modes will not appear in the isolated unit. Experimental testing on an isolated EDG unit will provide helpful insight into characterizing its failure modes.

Three acceleration-based limit states are used in a narrow acceleration range of [0.30–0.50 g]. The first limit state, EDG LS1, is the lower bound value of any possible EDG failure mode found in the literature [22–25,30,41]. The consensus is that a fix-based EDG unit should have at least an HCLPF equal to a PGA = 0.30 g.

Figure 14 shows the fragility curves for EDG LS1. The HCLPF value for the acceleration-based limit state is 0.99 g, represented by the blue dashed line. This result shows a 5% probability of failure given a horizontal PGA = 0.99 g. This failure is characterized by the lowest bound value of a fix-based EDG unit.

4.4.3. Results

Figure 15 presents the HCLPF in terms of the ground motion PGA for all limit states, including displacement- and acceleration-based EDPs. As shown previously, different HCLPF values were presented. These values were obtained assuming an uncertainty logarithmic standard deviation of $\beta_u = 0.30$ and varying values for the randomness logarithmic standard deviation of β_r. This parameter comes from the five ground motion triplets for each limit state with values ranging from 0.06 to 0.17. These values are recognized to be small for the ground motion set considered and increased to $\beta_r = 0.20$ to determine the HCLPF for every limit state.

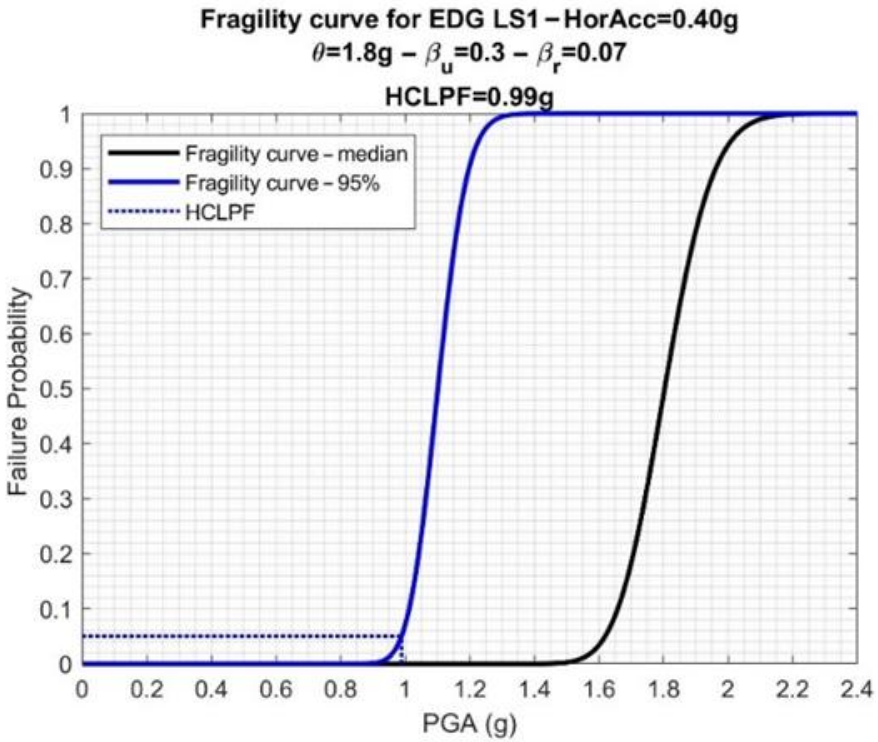

Figure 14. Fragility curve for EDG LS1—horizontal acceleration = 0.40 g.

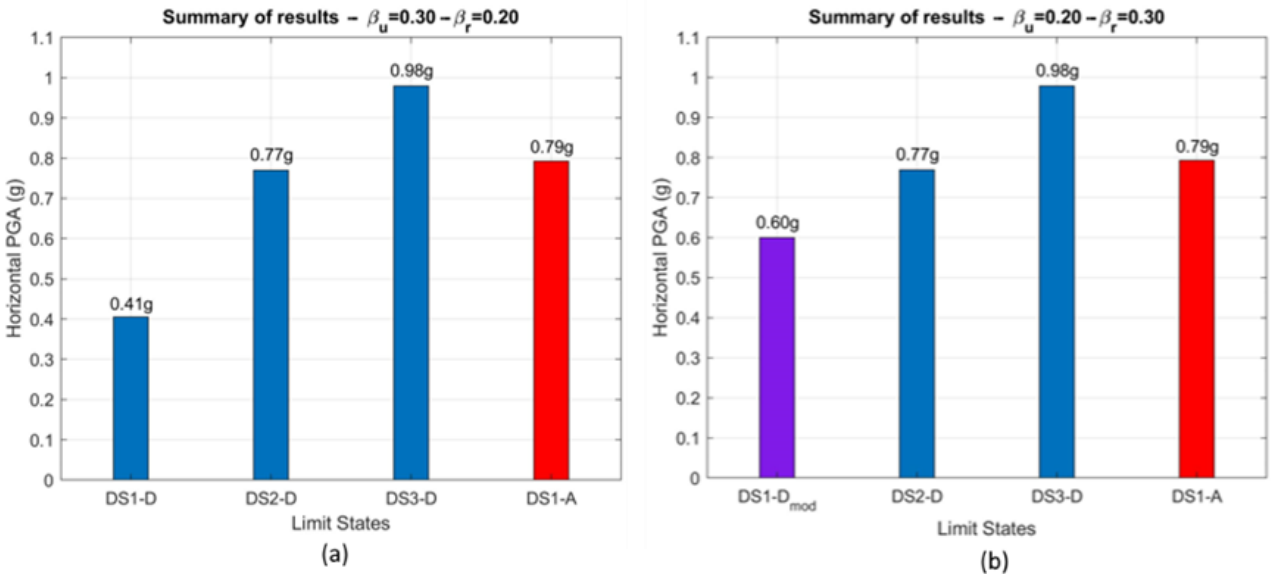

Figure 15. Fragility curves results for both limit states for (**a**) original pipeline LS (DS1-D), (**b**) modified pipeline LS (DS1-D_{mod}).

Figure 15a shows that the pipeline LS (DS1-D) limits the seismic protection system's performance. All other LS are above a PGA = 0.77 g, while the DS1-D is reached at PGA = 0.41 g. This PGA value would be the maximum horizontal PGA that the seismic protection system could experience with a 95% confidence of not exceeding the 5% probability of failure with no damage and linear behavior expected, as required by Design Category 5 (SDC-5) with an LS-D, according to ASCE/SEI-43-05 [21]. Figure 15b shows the results by modifying the pipeline LS (DS1-D_{mod}) at a limit equal to 224 mm, which represents a moderate damage state (equivalent to damage of broken meshes) [42]. The seismic protection system could perform at 146% of the previously defined maximum PGA.

Locations with a horizontal PGA up to 0.60 g could use the seismic protection system while complying with ASCE/SEI-43-05 [21] if the deformation capacity of the pipeline is 224 mm.

To equal the PGA required to reach the second displacement-based limit state (DS2-D), the pipeline's HCLPF should be 320 mm. This would allow the seismic protection system to satisfy the performance of places with a seismic hazard equal to PGA = 0.77 g (188% of the original maximum PGA). Providing a pipeline with a higher deformation capacity to cross the isolation interface with limited damage would enhance the system's performance.

5. Discussion

The proposed seismic isolation system satisfies the SDC-5 for the seismic hazard considered according to ASCE/SEI-43-05 [21], assuming a limit state LS-D, i.e., when no damage and elastic behavior is expected. The seismic hazard, characterized by the PGA, that the system could handle under the LS-D is 0.41 g. This is similar to a non-seismically isolated EDG and is based on having conventional pipelines. Detailing the pipelines to accommodate larger displacements is necessary to gain benefit from the isolation system. Conservative assumptions are made to be aligned and comply with the NPP safety standards. Experimental testing would provide a deeper insight into the EDG behavior when base-isolated, particularly the controlling failure mode and the behavior in the vertical direction. The minimum non-isolated EDG HCLPF was used for acceleration, which is a conservative assumption. Even under this assumption, the proposed system can withhold a PGA = 0.79 g assuming the scaled seismic hazard maintains its frequency content range used for design.

The probabilistic approach outcome shows its inherent conservatism compared to the deterministic approach. The same base isolation average lateral displacement of 127 mm, equivalent to the pipeline LSD-1, is used to compare the approaches. For the probabilistic approach, the PGA is 0.41 g for HCLPF, while the deterministic approach only considers the mean response with the PGA of 0.925 g. The probabilistic approach explicitly quantifies the failure probability, a feature the deterministic approach does not capture.

Including the vertical ground motion reduces the effectiveness of the proposed seismic protection system but still reduces the EDG acceleration. Quantifying the reduction in terms of the PGA shows an amplification around 0.20 times the PGA for the EDG acceleration when considering only the 2D horizontal acceleration. When using the 3D ground motion acceleration, a factor of 0.50 times the PGA is obtained.

This analysis shows that the pipeline deformation capacity is the controlling limit state. To be aligned with the LS-D criteria [21], the pipeline must be designed to accommodate the system lateral deformation under a controlled damage level. The metric required to characterize the pipeline deformation needs to be expressed as an HCLPF value for consistency. Experimental testing on flexible pipelines crossing the isolation interface would provide the necessary data to extend the proposed seismic protection system to areas with higher seismic hazards than PGA = 0.41 g.

Further studies are required to validate the proposed system under different seismic hazards and also consider the performance under operational loads not considered here. The two isolation levels need to be designed considering the local seismic hazard including expected frequency content for effective isolation performance.

6. Conclusions

The EDG seismic performance is critical to the operations of an NPP in the case of a loss of offsite power. The proposed seismic protection system can significantly increase safety margin compared to standard EDG support installation. Incorporating two isolation levels with distinct properties defined according to a specific seismic hazard allows the base isolated EDG to perform at a higher seismic demand, expressed in terms of PGA, with significant confidence of a low probability of failure and elastic behavior. The pipeline deformation capacity that crosses the isolation interface needs to be designed accordingly for the system to function effectively in larger seismic hazard region, i.e., larger horizontal PGAs.

Experimental testing on both a pipeline designed to accommodate the required lateral deformation and the isolated EDG unit failure modes are critical to validate the proposed seismic protection system.

The innovation of the proposed seismic protection system is in the use of two isolation levels to decouple the seismic demand and enables designers to combine existing and proven seismic protection devices. One isolation level focuses solely on the reduction of the horizontal component demand, while the second isolation level handles the vertical component. This approach maximizes the seismic reduction capabilities of each device. The enhanced seismic protection system can be tailored to specific seismic demands by changing a few parameters only for a decoupled seismic demand. The low probability of failure that this design adds to the standard EDG support solution could be a step forward to standardizing an EDG seismic protection system.

Author Contributions: Conceptualization, M.K. and G.M.; methodology, G.M.; software, R.B.; validation, G.M. and M.K.; investigation, R.B.; writing—original draft preparation, R.B.; writing—review and editing, G.M.; supervision, G.M. and M.K.; project administration, M.K.; funding acquisition, G.M. and M.K. All authors have read and agreed to the published version of the manuscript.

Funding: This research was funded by the National Research Foundation of Korea (NRF), grant number NRF-2017M2A8A4014829.

Acknowledgments: This study was supported by the National Research Foundation of Korea (NRF).

Conflicts of Interest: The authors declare no conflict of interest.

References

1. Ebisawa, K.; Ando, K.; Shibata, K. Progress of a research program on seismic base isolation of nuclear components. *Nucl. Eng. Des.* **2000**, *198*, 61–74. [CrossRef]
2. JAERI. *Characteristics and Dynamic Response Analysis of 3-D Component Base Isolation System Using Ball Bearings and Air Springs*; Japan Atomic Energy Research Institute: Tokyo, Japan, 2000.
3. Choun, Y.-S.; Kim, M.-K.; Ohtori, Y. The use of a base isolation system for an emergency diesel generator to reduce the core damage frequency caused by a seismic event. In Proceedings of the SMiRT 19, Toronto, ON, Canada, 12–17 August 2007; Volume 19, pp. 1–8.
4. Furukawa, S.; Sato, E.; Shi, Y.; Becker, T.; Nakashima, M. Full-scale shaking table test of a base-isolated medical facility subjected to vertical motions. *Earthq. Eng. Struct. Dyn.* **2013**, *42*, 1931–1949. [CrossRef]
5. Najafijozani, M.; Becker, T.C.; Konstantinidis, D. Evaluating adaptive vertical seismic isolation for equipment in nuclear power plants. *Nucl. Eng. Des.* **2020**, *358*, 110399. [CrossRef]
6. Kumar, M.; Whittaker, A.S.; Constantinou, M.C. Seismic isolation of nuclear power plants. *Nucl. Eng. Technol.* **2015**, *46*, 569–580. [CrossRef]
7. Medel-Vera, C.; Ji, T. Seismic protection technology for nuclear power plants: A systematic review. *J. Nucl. Sci. Technol.* **2015**, *52*, 607–632. [CrossRef]
8. Tsutsumi, H.; Ebisawa, K.; Suzuki, M.; Yamada, H.; Fujimoto, S. Development of the Methodology for Evaluating the Probability of Failure of Seismic Isolation System for Nuclear Components. In Proceedings of the SMiRT, Manchester, UK, 10–14 August 2015.
9. Inoue, K.; Fushimi, M.; Moro, S.; Morishita, M.; Kitamura, S.; Fujita, T. Development of Three-Dimensional Seismic Isolation System for Next Generation Nuclear Power Plant. In Proceedings of the 13th World Conference on Earthquake Engineering, Vancouver, BC, Canada, 1–6 August 2004. No. 1537.
10. Suhara, J.; Tamura, T.; Ohta, K.; Okada, Y.; Moro, S. Research on 3-D Base Isolation System Applied to New Power Reactor 3-D Seismic Isolation Device with Rolling Seal Type Air Spring: Part 1. In Proceedings of the Transactions of the 17th International Conference on Structural Mechanics in Reactor Technology (SMiRT 17), Prague, Czech Republic, 17–22 August 2003; pp. 1–6.
11. Nawrotzki, P.; Siepe, D. Structural challenges of power plants in high seismic areas. In Proceedings of the Second European Conference on Earthquake Engineering and Seismology, Istanbul, Turkey, 25–29 August 2014; pp. 25–29.
12. Choun, Y.; Kim, M.; Seo, J. Seismic and Vibration Isolation of an Emergency Diesel Generator by Using a Spring-Viscous Damper System. In Proceedings of the SMiRT 19, Toronto, ON, Canada, 12–17 August 2007; p. 8.
13. Kančev, D.; Duchac, A.; European Commission; Joint Research Centre; Institute for Energy and Transport. *European Clearinghouse: Events Related to Emergency Diesel Generators*; Publications Office of the European Union: Luxembourg, 2013.
14. Gregory, N.; Simon, R.; Branden, D.; Kermin, C. Practical Implementation of ASCE-41 and NLRHA Procedures for the Design of the LLUMC Replacement Hospital. In Proceedings of the 2017 SEAOC Conference Proceedings, San Diego, CA, USA, 13–15 September 2017; pp. 1–8.

15. Tomizawa, T.; Takahashi, O.; Suhara, J.; Okada, K.; Tsuyuki, Y.; Fujita, T. Vibration test in a building named ' Chisuikan' using three-dimensional seismic isolation system. In Proceedings of the ISEC 2013—7th International Structural Engineering and Construction Conference: New Developments in Structural Engineering and Construction, Honolulu, HI, USA, 18–23 June 2013; pp. 791–796. [CrossRef]
16. Vamvatsikos, D.; Cornell, C.A. Incremental dynamic analysis. *Earthq. Eng. Struct. Dyn.* **2002**, *31*, 491–514. [CrossRef]
17. Budnitz, R.J. Current status of methodologies for seismic probabilistic safety analysis. *Reliab. Eng. Syst. Saf.* **1998**, *62*, 71–88. [CrossRef]
18. DIS. DIS 3D Isolation System. Available online: http://dis-inc.com/pdf_files/DIS%203D%20Isolation%20Systems.pdf (accessed on 15 October 2020).
19. KAERI. *Generation of Input Ground Acceleration for Analysis of Nuclear Plant Structures Reflecting Site Characteristics in Korea*; KAERI: Pusan, Korea, 2018.
20. Choi, I.-K.; Nakajima, M.; Choun, Y.-S.; Ohtori, Y. Development of the site-specific uniform hazard spectra for Korean nuclear power plant sites. *Nucl. Eng. Des.* **2009**, *239*, 790–799. [CrossRef]
21. *ASCE43-05*; Seismic Design Criteria for Structures, System, and Components in Nuclear Facilities. American Society of Civil Engineers: Reston, VA, USA, 2006.
22. U.S. Nuclear Regulatory Commission. *NUREG/CR-4334—An Approach to the Quantification of Seismic Margins in Nuclear Power Plants*; U.S. Nuclear Regulatory Commission: Rockville, MD, USA, 1985.
23. U.S. Nuclear Regulatory Commission. *Risk Assessment Standardization Project (RASP) Handbook-External Events: Seismic Event Modeling and Seismic Risk Quantification Seismic Event Modeling and Seismic Risk Quantification*; U.S. Nuclear Regulatory Commission: Rockville, MD, USA, 2017.
24. Liu, W.; Aziz, T.S. Seismic Capacity of Emergency Power Supply Diesel Generator Set for Candu 6. In Proceedings of the SMiRT 19, Toronto, ON, Canada, 12–17 August 2007; pp. 1–8.
25. Jeong, Y.S.; Baek, E.R.; Jeon, B.G.; Chang, S.J.; Park, D.-U. Seismic performance of emergency diesel generator for high frequency motions. *Nucl. Eng. Technol.* **2019**, *51*, 1470–1476. [CrossRef]
26. Jeon, B.-G.; Choi, H.-S.; Hahm, D.-G. Seismic Fragility Estimates of Piping System of Base-isolated Nuclear Power Plant. In Proceedings of the Transactions of the 17th International Conference on Structural Mechanics in Reactor Technology (SMiRT 23), Manchester, UK, 10–14 August 2015; pp. 1–10.
27. JNES. *Proposal of Technical Review Guidelines for Structures with Seismic Isolation*; JNES: Tokyo, Japan, 2013.
28. Touboul, F.; Sollogoub, P.; Blay, N. Seismic behaviour of piping systems with and without defects: Experimental and numerical evaluations. *Nucl. Eng. Des.* **1999**, *192*, 243–260. [CrossRef]
29. Zhang, T.; Brust, F.W.; Wilkowski, G.; Shim, D.-J.; Nie, J.; Hofmayer, C.H.; Ali, S.A. Analysis of JNES seismic tests on degraded piping. In Proceedings of the Pressure Vessels and Piping Conference, Bellevue, WA, USA, 18–22 July 2010. [CrossRef]
30. Choun, Y.S.; Kim, M.K. A performance assessment of a base isolation system for an emergency diesel generator in a nuclear power plant. *Nucl. Eng. Technol.* **2008**, *40*, 285–298. [CrossRef]
31. Kawakami, K.; Hara, S.; Shibata, F.; Ohno, H.; Horimizu, T.; Ichimashi, Y.; Uchiyama, I.; Niino, Y.; Takayanagi, T.; Kajimura, M.; et al. Seismic Proving Test of Emergency Diesel Generator System. In Proceedings of the SMiRT, Stuttgart, Germany, 15–20 August 1993.
32. Kim, M.K.; Choun, Y.S.; Seo, J.M. Demonstration of the vibration control performance of coil spring-viscous damper systems by measuring the vibration of an emergency diesel generator. *JVC J. Vib. Control* **2010**, *16*, 207–229. [CrossRef]
33. FEMA. *FEMA P-751—NEHRP Recommended Seismic Provisions for New Buildings and Other Structures*; FEMA: New York, NY, USA, 2009.
34. Christopoulos, C.; Filiatrault, A. *Principles of Passive Supplemental Damping and Seismic Isolation*; IUSS Press: Pavia, Italy, 2006; Volume 133, p. 1192.
35. Kelly, J.M.; Konstantinidis, D.A. *Mechanics of Rubber Bearings for Seismic and Vibration Isolation*; Wiley: Chichester, UK, 2011.
36. Naeim, F.; Kelly, J.M. *Design of Seismic Isolated Structures: From Theory to Practice*; Wiley: Chichester, UK, 1999.
37. PEER. *OpenSees: A Framework for Earthquake Engineering Simulation*; University of California: Berkeley, CA, USA, 2020.
38. Kafali, C.; Grigoriu, M. Seismic fragility analysis: Application to simple linear and nonlinear systems. *Earthq. Eng. Struct. Dyn.* **2007**, *36*, 1885–1900. [CrossRef]
39. Zhao, C.; Yu, N.; Peng, T. Probabilistic seismic fragility assessment of isolated nuclear power plant structure using IDA and MSA methods. *Structures* **2021**, *34*, 1300–1311. [CrossRef]
40. Pang, R.; Xu, B.; Zhou, Y.; Song, L. Seismic time-history response and system reliability analysis of slopes considering uncertainty of multi-parameters and earthquake excitations. *Comput. Geotech.* **2021**, *136*, 104245. [CrossRef]
41. Prassinos, P.G.; Murray, R.C.; Cummings, G.E. *Seismic Margin Review of the Maine Yankee Atomic Power Station*; Lawrence Livermore National Laboratory: Livermore, CA, USA, 1987; Volume 1.
42. Shang, Q.; Wang, T.; Li, J. Seismic fragility of flexible pipeline connections in a base isolated medical building. *Earthq. Eng. Eng. Vib.* **2019**, *18*, 903–916. [CrossRef]